

Final states of the two dimensional electron plasma trapped in magnetic field

Ryo KAWAHARA^{*} and Hiizu NAKANISHI[†]

Department of Physics, Kyushu University 33, Fukuoka 812-8581.

(Received May 24, 2019)

We have performed numerical simulations on the pure electron plasma system under strong magnetic field, in order to examine final states that the system eventually evolves into. We use ring states as the initial states changing the width and find that the system evolves into a vortex crystal state from a thinner ring state while a state with a single-peaked density distribution is obtained from a thicker ring initial state. We compare our results with experiments and some statistical theories, which includes the Gibbs-Boltzmann statistics, Tsallis statistics, the fluid entropy theory, and the minimum enstrophy state. From some of those initial states, we obtain the final states which are close to the minimum enstrophy state, but we also find that the final states depend upon initial states, even if the initial states have the same energy and angular momentum, which means the ergodicity does not hold.

KEYWORDS: non-neutral plasma, two-dimensional turbulence, numerical simulation, long range force, non-extensive system,

1. Introduction

A system with long range interaction behaves quite differently from that with short range interaction because the total energy is not proportional to the system size and the thermodynamic limit cannot be defined in an ordinary sense. In such a case, even a small subsystem of a large system may not obey the Boltzmann statistics because the subsystem interacts strongly with the rest of the system and its energy depends on the size of the whole system.

An example of such systems is the pure electron plasma, where the electrons interact via the Coulomb law. By applying strong magnetic field to the system, one can confine the electrons in a container for quite a long time, and examine final states of the system.

The system can be described by two dimensional (2-d) Euler equation with the vorticity of same sign if the cyclotron motion is ignored, thus its dynamics is analogous to that of 2-d incompressible inviscid fluid. In the 2-d fluid systems, dynamics of vortices are known to be important to understand the system behavior, as is seen in large scale geophysical flows of high Reynolds number.

Statistical theories of the 2-d perfect fluid originate from Onsager's work for point vortex model.¹⁾ Since this model is described by a Hamiltonian, he has introduced the "temperature" in microcanonical ensemble through the derivative of the logarithm of the number of states with respect to the total energy. Especially, in the case of "negative temperature", this theory predicts that small vortices merge together and eventually self-organize into a large single cluster.

In some simulations, the connection between the point vortex system and the Onsager's theory have been investigated, and the result shows that, for the three particle case, the initial state in the negative temperature region leads to chaotic motion of particles.²⁾ Related result that

the sign of the temperature affects the dynamics of the system has been also obtained for the system which contains particles with both signs.³⁾

Since Onsager, many theories have been proposed so far.⁴⁾ Some of them are based on maximization of the entropy,⁵⁻⁸⁾ while others are based on minimization of the enstrophy.⁹⁾ Most of the theories predict the formation of a large single cluster as the equilibrium state. However, experimental test of the theories are difficult with actual 2-d fluid, and the 2-d electron plasma system can be used to test such theories.

In 1994, an experiment has been performed by Huang and Driscoll using 2-d electron plasma,¹⁰⁾ which suggests that the stationary state of the 2-d electron plasma system is described by the minimum enstrophy theory and cannot be explained by any of the maximum entropy theories. This is particularly interesting because the minimum enstrophy state has been shown to be the maximum Tsallis entropy state with $q = 1/2$ in the Tsallis statistics, which has been developed to describe non-extensive systems.¹¹⁾

Numerical simulations on the 2-d electron plasma system have been also performed. The minimum enstrophy state is also observed in simulational study using the initial states which are same with those in the experiment.¹²⁾ However, initial state dependence of such stationary state has not been tested systematically.

Another kind of final state that is called vortex crystal state, has been found in experiments.^{13,14)} The vortex crystal is analogous to the coherent vortex structure in 2-d turbulent flow,¹⁵⁾ but the vortex crystal states has not been described by any known statistical theories; it is described only phenomenologically.¹⁶⁾

In numerical simulations, the existence of vortex crystal state is confirmed and the relaxation process to it has been studied. It has been shown that the vortex crystal state is sensitive to the small difference in initial states, and background vortices stabilize the vortex

^{*}E-mail : ryokawa@stat.phys.kyushu-u.ac.jp

[†]E-mail : naka4scn@mbox.nc.kyushu-u.ac.jp

crystal state.¹⁷⁾ The vortex crystal state is realized not only with large number of particles but also with only several hundred particles. In the simulation, interaction between vortex clumps and background vortices is also found to be important; there are exchange of energy and particles between them even after the formation of the vortex crystal state.²⁾ Effects of background vortices in the vortex crystal state, such as dynamics of clumps and formation of regular structure, have been also intensively studied in experiments.^{18–20)}

In this paper, we study the final states of the two-dimensional pure electron plasma under the strong magnetic field by numerical simulation. With our numerical results, we examine a several statistical theories for the stationary state.

The paper is organized as follows: in §2, we introduce the 2-d electron plasma system under magnetic field and define a model. In §3, we briefly review some statistical theories. Simulation method and results are described in comparison with the statistical theories in §4, and summary and discussion are given in §5.

2. Model system and its behavior

The system we consider is a pure electron plasma system in a cylindrical container with the uniform external magnetic field along its axis; in a certain experimental situation,^{10, 13, 14)} the system behaves like a 2-d one in the plane perpendicular to the axis, in which situation we investigate in the following.

2.1 Equations of motion

We assume that the magnetic field is strong enough that the radii of cyclotron motion can be ignored, then the electron velocity \mathbf{v} within the plane is given by the drift velocity of guiding center

$$\mathbf{v} = \frac{\mathbf{E} \times \mathbf{B}}{B^2} \quad (1)$$

under the existence of the electronic field \mathbf{E} perpendicular to the magnetic field \mathbf{B} . In the present situation, \mathbf{E} is generated by the electron themselves, thus the electrons do not repel each other and the plasma can be confined in a container (Malmberg trap, Fig. 1). Then, the density field $n(x, y)$, the velocity field $\mathbf{v}(x, y)$, and the electro-static potential $\phi(x, y)$ in 2-d follows

$$\frac{Dn}{Dt} \equiv \frac{\partial n}{\partial t} + \mathbf{v} \cdot \nabla n = 0, \quad (2)$$

$$\mathbf{v} = \hat{\mathbf{z}} \times \nabla \phi = \left(-\frac{\partial \phi}{\partial y}, \frac{\partial \phi}{\partial x} \right), \quad (3)$$

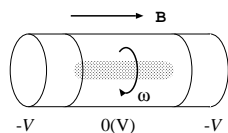


Fig. 1. Schematic diagram of Malmberg trap of pure electron plasma.

$$\nabla^2 \phi = n, \quad (4)$$

where $\hat{\mathbf{z}}$ denotes the unit vector perpendicular to the plane and ∇ is the 2-d nabla. The boundary condition at the container wall is given by $\phi = 0$. We have normalized the potential and density as $(1/B)\phi \mapsto \phi$ and $(e/\epsilon_0 B)n \mapsto n$ where e is the charge of an electron and ϵ_0 is the dielectric constant of vacuum.

It can be shown that the density field n equals to the vorticity $\omega(\mathbf{r}) \equiv (\nabla \times \mathbf{v})_z$ of the 2-d velocity field \mathbf{v} and the velocity field \mathbf{v} is solenoidal ($\nabla \cdot \mathbf{v} = 0$), therefore, the set of equations (2) - (4) is the same with that of Euler equation for the 2-d incompressible inviscid fluid with free slip boundary condition, but the vorticity takes only positive value in the present system.

Although the dynamics considered is not Newtonian, it can be expressed in terms of Hamiltonian,

$$\frac{dx_i}{dt} = \frac{\partial H}{\partial y_i}, \quad \frac{dy_i}{dt} = -\frac{\partial H}{\partial x_i}. \quad (5)$$

The Hamiltonian H is given by

$$\begin{aligned} H &= -\frac{1}{2} \sum_i^N \sum_{j \neq i}^N G(\mathbf{r}_i, \mathbf{r}_j) - \frac{1}{2} \sum_i^N G_m(\mathbf{r}_i, \mathbf{r}_i) \\ &= -\frac{1}{2} \sum_i^N \phi_i(\mathbf{r}_i), \end{aligned} \quad (6)$$

where $G(\mathbf{r}_i, \mathbf{r}_j)$ is the 2-d Green function for the electric potential, $G_m(\mathbf{r}, \mathbf{r}')$ is the electric potential at \mathbf{r} by the mirror charge induced by the charge at \mathbf{r}' to satisfy the boundary condition, and $\phi_i(\mathbf{r})$ is the electric potential due to all the electrons except for the i -th. The Green function satisfies

$$\nabla^2 G(\mathbf{r}, \mathbf{r}') = \delta(\mathbf{r} - \mathbf{r}'), \quad (7)$$

under an appropriate boundary condition. In the present case, we consider that the system is in a cylindrical container with the radius R_w , then ϕ_i is given by²⁾

$$\begin{aligned} \phi_i(\mathbf{r}) &\equiv + \frac{1}{2\pi} \sum_{j \neq i}^N \ln |z - z_j| \\ &\quad - \frac{1}{2\pi} \sum_j^N \left[\ln |z - \frac{R_w^2}{z_j^*}| + \ln \frac{|z_j|}{R_w} \right], \end{aligned} \quad (8)$$

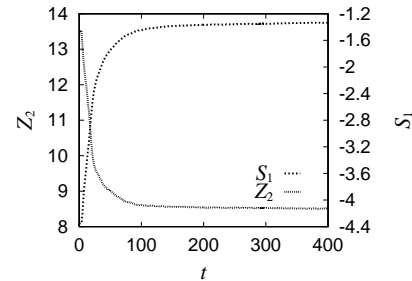


Fig. 2. Time evolution of two Casimirs in the simulation: the dotted line and the dashed line represent the enstrophy Z_2 and the entropy S_1 , respectively.

with $z = x + iy$ and z^* is the complex conjugate of z ; the second term corresponds to the potential by the mirror charges.

2.2 Constants of the dynamics

The Hamiltonian H is a constant of the dynamics and is expressed as

$$\begin{aligned} H &= -\frac{1}{2} \int d^2\mathbf{r} \int d^2\mathbf{r}' n(\mathbf{r})n(\mathbf{r}')G(\mathbf{r}, \mathbf{r}') \\ &= -\frac{1}{2} \int d^2\mathbf{r} n(\mathbf{r})\phi(\mathbf{r}) \\ &= \int d^2\mathbf{r} \frac{1}{2}\mathbf{v}^2(\mathbf{r}), \end{aligned} \quad (9)$$

which corresponds to the total energy.

In the case of system with the circular symmetry, the total angular momentum L around the center of the system,

$$L \equiv \int d^2\mathbf{r} (\mathbf{r} \times \mathbf{v}(\mathbf{r}))_z = \int d^2\mathbf{r} r^2 n(\mathbf{r}), \quad (10)$$

is also a constant of the dynamics.

In addition to the above two quantities, it can be shown that the integral Z of any function f of n ,

$$Z \equiv \int d^2\mathbf{r} f(n(\mathbf{r})), \quad (11)$$

is a constant of dynamics; this is called a Casimir constant.^{11,21)} Although any Casimir is a conserved quantity for the dynamics given by eq.(2), it is often not conserved in simulations and experiments (Fig.2(b)); this is because the field quantities are defined only in a finite resolution in space.

Out of Casimirs, the enstrophy Z_2 ,

$$Z_2 \equiv \frac{1}{2} \int d^2\mathbf{r} n^2(\mathbf{r}), \quad (12)$$

and the one-body entropy S_1 ,

$$S_1 = - \int d^2\mathbf{r} n(\mathbf{r}) \log n(\mathbf{r}), \quad (13)$$

are of particular interest.

2.3 Stability and evolution of states

It can be shown that the rotationally symmetric state with a decreasing density n as a function of r is not linearly unstable and is numerically stable. On the other hand, the ring state, where the electrons are distributed in a ring shape region, is linearly unstable, and the instability is called diocotron instability.²²⁾

Fig. 3 shows two examples of time sequences which start from unstable initial states and lead to two types of final states; the sequence in Fig.3(a) starts from a single ring configuration, which destabilizes by the mode three, eventually falls into a singly peaked stable density distribution. In the case of Fig.3(b), a double ring initial configuration results in instability by a higher mode to break into many vortices, which merge occasionally while they undergo a collective chaotic motion, and eventually several vortices that survive form a regular structure, which does not undergo further change during our simu-

lation time; this state is called a vortex crystal state.¹³⁾

3. Statistical theories for final states

Although the dynamics of the present system is highly nonlinear and unpredictable, final steady states may be predicted by a simple principle; actually, there have been several statistical theories developed to predict the vortex cluster as a final state using variational methods.⁴⁾ We briefly review some of them in this section.

3.1 Maximum one-body entropy state

Although the one-body entropy S_1 (eq.(13)) is a Casimir constant, in actual simulations, it shows rapid initial increase and reaches a steady value, (Fig.2) thus the density distribution n of the steady state might be given by maximizing S_1 , keeping the total number of electron N , the total energy H , and the total angular momentum L constant. Using variational method,

$$\delta(S_1 - aN - bH - cL) = 0, \quad (14)$$

where a, b and c are Lagrange multipliers and determined from the constraints.¹⁰⁾ If the energy H in eq.(9) is evaluated ignoring electron correlation, then we obtain

$$n(\mathbf{r}) = \exp(-1 - a + b\phi(\mathbf{r}) - cr^2). \quad (15)$$

From eq.(4), ϕ satisfies

$$\nabla^2\phi(\mathbf{r}) = \exp(-1 - a + b\phi(\mathbf{r}) - cr^2), \quad (16)$$

which can be solved numerically.

3.2 Maximum fluid entropy state

The fluid entropy^{7,8,23)} is the entropy defined in terms of the probability distribution $p(\sigma_j; \mathbf{r}_i)$ of the discretized vorticity σ_j in the coarse grained cell at \mathbf{r}_i as

$$S_{\text{fluid}} \equiv - \sum_{\mathbf{r}_i} \sum_{\sigma_j} p(\sigma_j; \mathbf{r}_i) \ln p(\sigma_j; \mathbf{r}_i), \quad (17)$$

where σ_j 's are strengths of microscopic vortex elements. This fluid entropy has been introduced based on the idea of counting the number of configurations of vortices over discretized space.²³⁾

The probability distribution $p(\sigma_j; \mathbf{r}_i)$ satisfies the normalization

$$\sum_{\sigma_j} p(\sigma_j; \mathbf{r}_i) = 1 \quad (18)$$

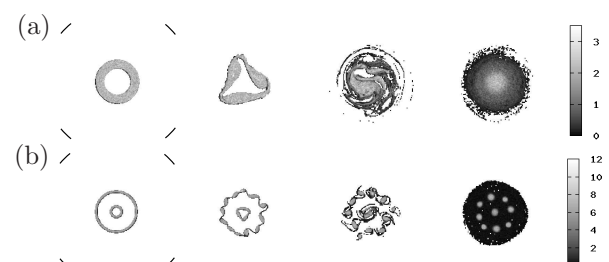


Fig. 3. Time evolutions of electron density distribution from a single ring initial state (a), and a double ring initial state (b). Initial distributions are shown in the left-most figures and final states are shown in the right-most figures. The conductor wall boundary is expressed by the black curve in the left-most figure.

at each \mathbf{r}_i , and is related with the total numbers of vortices $g(\sigma_j)$ of the strength σ_j by

$$g(\sigma_j) = \sum_{\mathbf{r}_i} p(\sigma_j; \mathbf{r}_i); \quad (19)$$

it is assumed that $g(\sigma_j)$ does not change because the strength of each vortex does not change.

The coarse grained density (vorticity) $n(\mathbf{r}_i)$ at the cell \mathbf{r}_i is given by

$$n(\mathbf{r}_i) = \sum_{\sigma_j} p(\sigma_j; \mathbf{r}_i) \sigma_j. \quad (20)$$

The maximum fluid entropy state is given by maximizing eq.(17) over variation of $p(\sigma_j; \mathbf{r}_i)$ under the constraints of eqs.(18) and (19) in addition to H and L . This gives

$$p(\sigma_j; \mathbf{r}_i) = \frac{\exp[-\gamma(\sigma_j) + b\phi(\mathbf{r}_i) - cr_i^2]}{\sum_{\sigma_k} \exp[-\gamma(\sigma_k) + b\phi(\mathbf{r}_i) - cr_i^2]}, \quad (21)$$

where $\gamma(\sigma_j)$, b and c are Lagrange multipliers. Note that the total number of particles N are given by

$$N = \sum_{\sigma_i \neq 0} g(\sigma_i), \quad (22)$$

therefore, we need not include N as a constraint. In the continuum limit in space, combining this with eqs.(20) and (4), the potential ϕ can be solved numerically.

In principle, these constants and the values of σ_j 's should be determined by initial states of 2-d fluid. However, there is ambiguity in the values of σ_j 's since we only know the coarse grained information of the initial states, $n(\mathbf{r})$, and different sets of σ_j 's can give the same $n(\mathbf{r})$. To apply the theory to our simulation of 2-d electron plasma, we take the values of σ_j 's to be those of the coarse grained density of the initial states, as Huang and Driscoll did in their analysis of the experiment.¹⁰⁾

3.3 Minimum enstrophy state

Another Casimir constant, the enstrophy Z_2 defined by eq.(12) is known to cascade towards smaller length scales,^{24,25)} and dissipated in the regime where eqs.(2) is not exact; numerically, the enstrophy has been shown to decrease initially until it reaches a steady value, thus n for the steady states could be given by minimizing Z_2 within given values of N , H and L as in the maximum entropy state.^{9,10)} This gives

$$n(\mathbf{r}) = a - b\phi(\mathbf{r}) + cr^2, \quad (23)$$

where a , b , and c are again the Lagrange multipliers and determined by the constraints. Operating the 2-d Laplacian on both hand sides of the eq.(23) and assuming $n(\mathbf{r})$ is axisymmetric, we obtain

$$\frac{d^2n}{dr^2} + \frac{1}{r} \frac{dn}{dr} + bn - 4c = 0. \quad (24)$$

This is the 0-th order Bessel equation, therefore the solution is given by the Bessel function, but the density $n(\mathbf{r})$ cannot take negative values. For $b > 0$, which corresponds with the higher energy case, we employ the so-

lution

$$n(r) = \begin{cases} \alpha[J_0(\beta r) - J_0(\beta r_0)], & (r < r_0) \\ 0, & (r_0 < r) \end{cases} \quad (25)$$

where $J_0(x)$ is the 0-th order Bessel function, and α , β , and r_0 are determined by the constraints. The parameter r_0 is a cutoff length, which is introduced to avoid negative density region.^{9,10)} For $b < 0$ (the lower energy case), the solution is

$$n(r) = \begin{cases} \alpha[I_0(\beta r) - I_0(\beta r_0)], & (r < r_0) \\ 0, & (r_0 < r) \end{cases} \quad (26)$$

where $I_0(x) = J_0(ix)$ is the 0-th order modified Bessel function. This solution gives the pancake shape of $n(\mathbf{r})$ in the limit of $\beta \rightarrow \infty$ ($\alpha < 0$), which corresponds to the minimum energy state.

Actually, it has been shown experimentally that there are some cases where final states are very close to the minimum enstrophy states.¹⁰⁾

It has been pointed out that the minimum enstrophy state is the state that maximizes Tsallis entropy

$$S_q = \frac{1}{1-q} \int d^2\mathbf{r} [p^q(\mathbf{r}) - p(\mathbf{r})] \quad (27)$$

with $q = 1/2$ in the Tsallis statistics formalism.¹¹⁾

4. Simulations

4.1 Method

We simulate the system using a variation of the point vortex method;²⁶⁾ for a given set of electron (or vortex) positions, we calculate the electron density $n(\mathbf{r})$ on a grid points by averaging over the cell, then Poisson equation is solved to obtain the electro-static potential $\phi(\mathbf{r})$, from which the electric field $\mathbf{E}(\mathbf{r})$ is calculated, and the electron positions are updated by eq.(3); this is called the vortex-in-cell simulation.^{17,27)} Numerical integration in time is performed using the second-order Adams-Bashforth-Adams-Moulton method and Poisson's equation is solved by an implicit method adopting multiple grids to accelerate the convergence.²⁸⁾

The following simulations are performed on the grid 256×256 or 512×512 with the particle number $N = 80 \times 10^3$.

4.2 Results

4.2.1 General trends and classification of final states

We have systematically examined final states in the case where the system starts from the ring states with various ring width (Fig.4(a)); the initial ring state is the state where the electrons are distributed uniformly in the region $r \in [R_1, R_0]$, and the ratio R_1/R_0 is changed from

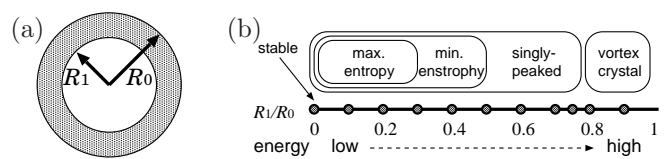


Fig. 4. (a) Initial ring state. (b) Schematic diagram of the final states for various ring width R_1/R_0 .

0 to 1. The total number of electron N and the angular momentum L are fixed to $N = 80 \times 10^3$ and $L = \pi/2$ for all cases, but the energy H is an increasing function of R_1/R_0 , namely, the energy is larger for the narrower ring.

The results are summarized in Fig.4(b).

In the case of the narrower ring initial state with $0.8 \lesssim R_1/R_0 \leq 1$, after the diocotron instability, the system goes through the chaotic motion of electron clumps; they merge occasionally and finally result in the vortex crystal state, which does not change any more. The number of clumps in the final state is very sensitive to the initial configuration because the clumps merges accidentally during chaotic motion; their final number depends even upon microscopic positions of electron in the initial states.

For smaller value of $R_1/R_0 \lesssim 0.8$, the final states are singly peaked stationary states with the circular symmetry; in this regime, the final state is rather insensitive to detail of the initial state and does not depend upon the microscopic configuration. As the ratio R_1/R_0 decreases, the density distribution of the final state becomes flatter around the peak at the center, as can be seen in Fig.5, and the initial “pancake state” with $R_1/R_0 = 0$ is stable and the system does not evolve at all.

For $R_1/R_0 \lesssim 0.5$, the minimum enstrophy state seems to give a reasonably good description of the final stationary state (Fig.5(b)), and for $R_1/R_0 \lesssim 0.3$, the minimum enstrophy state and the maximum entropy state are not so different and both of them are not very far from the final state obtained from the simulations. (Fig.5(a))

Note that the minimum enstrophy state has no physical solution with the present angular momentum for $R_1/R_0 \gtrsim 0.5$.¹⁰⁾

Actually, for $R_1/R_0 \approx 0$, all the statistical theories give the states that resemble each other very much and cannot be distinguished clearly; this is the result of the fact that, for $R_1/R_0 = 0$, the only possible state for the given energy and angular momentum is the initial pancake state, thus all the statistical theories should give the same state with this initial state.

The minimum enstrophy state seems to give a better approximate state for $0.3 \lesssim R_1/R_0 \lesssim 0.5$ than the maximum entropy state. This is because the simulations give the final state with a steeper peak for larger R_1/R_0 and the minimum enstrophy state tends to give the state

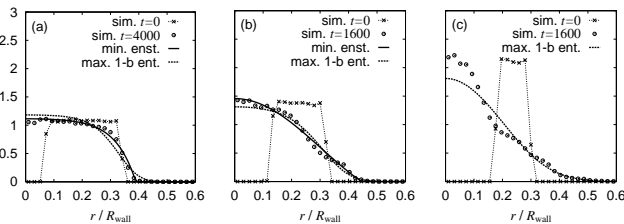


Fig. 5. The radial density distributions for the stationary states from the ring initial states with $R_1/R_0 = 0.2$ (a), 0.4 (b) and 0.6 (c). The minimum enstrophy state and the maximum one-body entropy state are also shown except for $R_1/R_0 = 0.6$ (c), where no physical solutions of the minimum enstrophy state exists.

with steeper peak in n than the maximum entropy state. (Fig.5(b) and (c))

On the other hand, it should be noted that there is a discrepancy between the minimum enstrophy states and the stationary states obtained by the simulations, if one compares them carefully; in the minimum enstrophy state, the tail of the density profile is cut off with a finite slope at a certain point, beyond which the density is zero, while in the simulations, the density goes to zero smoothly with the zero slope.

4.2.2 Ergodicity

Although the minimum enstrophy state generally gives a reasonable description for $R_1/R_0 \lesssim 0.5$ in the case of ring initial state, the system does not have the ergodicity within the states of the given energy and angular momentum.

This can be seen in Fig.6, which shows the final stationary states and the states given by the statistical theories for the two initial states with the same values of N , L and H , namely, the single ring initial state with a finite density inside the ring (Fig.6(a)), and the double ring initial state (Fig.6(b)).

When we try to fit these states to the ones from the statistical theories, we should note that the maximum one-body entropy states and the minimum enstrophy states are same for the two cases because they only depend on the values of N , L and H . The final states by the simulations are clearly different, and the one from the single ring-like state almost coincides with the minimum enstrophy state, while the final state from the double ring is different from both of the maximum entropy and the minimum enstrophy states mainly because of the steep peak at the center.

In order to see if there are any statistical theories to fit the final states from the double ring, we try the maximum fluid entropy state and the maximum Tsallis entropy state, because these theories contains extra parameters other than the energy and the angular momentum, therefore, may be capable to distinguish the two initial

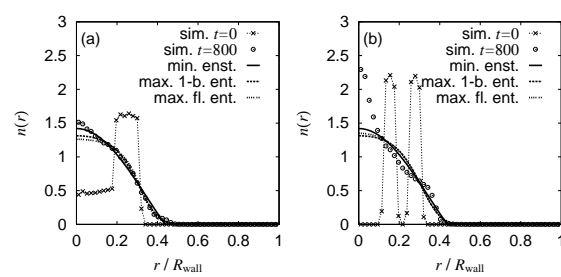


Fig. 6. Two different final states from two different initial states with the same energy $H = 2.078$ and the angular momentum $L = \pi/2$: The initial states are the single ring with a finite interior density (a) and the double ring (b). The minimum enstrophy state, the maximum one-body entropy state and the maximum fluid entropy state are also shown; they are the same for both cases except for the maximum fluid entropy states; the maximum fluid entropy depends on the set of values σ_j , which is different for the two cases: $\sigma_0 = 0$, $\sigma_1 = 0.49$ and $\sigma_2 = 1.62$ for (a), and $\sigma_0 = 0$ and $\sigma_1 = 2.25$ for (b).

states.

The maximum fluid entropy state depends on choice of a set of σ_j . In Fig.6, we use the values determined from the initial density as shown in the caption of Fig.6. The resulting state, however, does not agree well with either of the stationary states as can be seen in Fig.6.

Fig.7 shows the density profiles for the maximum Tsallis entropy states. The maximum Tsallis entropy state has a parameter q ; the state with $q = 1/2$ is the minimum enstrophy state and $q = 1$ is the maximum one-body entropy state. It can be seen that the state with smaller value of q , such as $q = 1/3$ state, shows a fatter profile and is not closer to the simulation data in Fig.6(b) than the $q = 1/2$ state, or the minimum enstrophy state. Actually, one can see that the state with $q \approx 0.53$ shows the steepest density profile, which turns out to be very close to the minimum enstrophy state. It has been shown³⁰⁾ that the peak density decreases monotonically as q increases in the parameter region $0.5 < q < 1.0$. Again, it is clear that we cannot fit the state to the maximum Tsallis entropy state with any choice of the parameter q .

4.2.3 Peak density in the final stationary state

The major reason that we cannot fit the stationary state from the double ring in Fig.6 to any statistical theories we tried is that there exists a high density region around the center. The value of the peak density in the final stationary state is approximately the same with that in the initial state. This property can be seen in other cases of Figs.5 and 6 and in almost all the simulations we have done.

From the time developments of the states, it is conceivable that, during the relaxation process, the initial density is kept in the region of the peak density. The peak density in final states is never larger than that of initial states.

The similar feature has been observed in vortex merger process in the two-dimensional free decaying turbulence, where the vortices of both charges exist.^{15, 29)}

5. Summary and discussion

We have performed the numerical simulations on the two-dimensional Euler equation with non-negative vorticity field, in order to study the final steady states of the pure electron plasma under the strong magnetic field, and have compared them with a several statistical the-

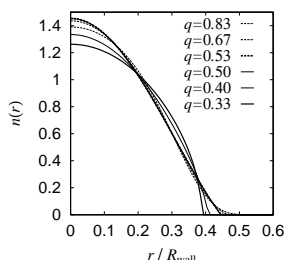


Fig. 7. Maximum Tsallis entropy states for various values of q with the same energy $H = 2.078$ and the angular momentum $L = \pi/2$, which corresponds to the parameters of Fig.6.

ories. By changing the radii ratio R_1/R_0 of initial ring state, we found (i) for $0.8 \lesssim R_1/R_0 \leq 1$, the final state is the vortex crystal state and (ii) for $0 \lesssim R_1/R_0 \leq 0.8$, the final state is the singly peaked state. Further study in the parameter region of singly peaked state revealed that (iii) for $0 \lesssim R_1/R_0 \leq 0.5$, the final singly peaked state is close to the minimum enstrophy state and (iv) for $0 \lesssim R_1/R_0 \leq 0.3$, the maximum entropy state and the minimum enstrophy state are close to each other, and the final steady state is close to both of them.

These are consistent with the experiment,¹⁰⁾ where the final state has been found very closed to the minimum enstrophy state when the initial state is prepared as the ring state.

Although these findings may look the evidence for that the minimum enstrophy state is good candidate for the statistical theory to describe the final state for some parameter region, we also have found that this system lacks the ergodicity, namely, the system does not necessarily fall into the same state even though its initial states have the same energy and angular momentum, thus the statistical theory gives the same state. In some experiments¹³⁾ and simulations,^{12, 17)} it has already been found that the vortex crystal state is sensitive to the microscopic difference in initial states and may lead to completely different final states. In the case where the final state is singly peaked, the final state is not sensitive to the microscopic details of the initial configuration, but we still found that the final state depends on macroscopic difference in the initial state, such as the single or double ring state.

As we have mentioned at §4.2.3, there is a tendency that the peak density of the initial state is conserved. This property, the conservation of the highest density, may be one of the reasons that the final state looks very close to the minimum enstrophy state for a certain parameter region because the parameter region where the minimum enstrophy state is seen seems to coincide with the parameter region where the highest density in the minimum enstrophy state is nearly equal to the highest density in the initial state. To clarify this point, further study is required.

Acknowledgments

We would like to thank to Professor Y. Kiwamoto, Professor M. Sakagami, Dr. Y. Yatsuyanagi and T. Yoshida for valuable discussions and comments.

- 1) L. Onsager: Supplemento, Nuova Cimento **6**, 8 (1949) 279 .
- 2) T. Yoshida and M. Sano: J. Phys. Soc. Jpn. **74** (2004) 587 .
- 3) Y. Yatsuyanagi, Y. Kiwamoto, H. Tomita, M.M. Sano, T. Yoshida, and T. Ebisuzaki: Phys. Rev. Lett. **94** (2005) 054502.
- 4) P. Tabeling: Physics Reports **362** (2002) 1 .
- 5) G. Joyce and D. Montgomery: J. Plasma Phys. **10** (1973) 107.
- 6) S. Kida: J. Phys. Soc. Jpn. **39** (1975) 1395 .
- 7) J. Miller, P. B. Weichman, and M. C. Cross: Phys. Rev. A **45** (1992) 2328 .
- 8) R. Robert and J. Sommeria: Phys. Rev. Lett. **69** (1992) 2776 .
- 9) C. E. Leith: Phys. Fluids **27** (1984) 1388 .
- 10) X.-P. Huang and C. F. Driscoll: Phys. Rev. Lett. **72** (1994) 2187.
- 11) B. M. Boghosian: Phys. Rev. E **53** (1996) 4754.

12) V. Pavlov, D. Buisine, and S. Decossin: *Phys. Fluids* **14** (2002) 3937 .

13) K.S. Fine, A.C. Cass, W.G. Flynn, and C.F. Driscoll: *Phys. Rev. Lett.* **75** (1995) 3277 .

14) C. F. Driscoll, D. Z. Jin, D. A. Schecter, E. J. Moreau, and D. H. E. Dubin: *Physica Scripta* **T84** (2000) 76 .

15) G. F. Carnevale, J. C. McWilliams, Y. Pomeau, J. B. Weiss, and W. R. Young: *Phys. Rev. Lett.* **66** (1991) 2735 .

16) D. Z. Jin and D. H. E. Dubin: *Phys. Rev. Lett.* **80** (1998) 4434 .

17) D. A. Schecter, D. H. E. Dubin, K. S. Fine, and C. F. Driscoll: *Phys. Fluids* **11** (1999) 905 .

18) A. Sanpei, Y. Kiwamoto, K. Ito, and Y. Soga: *Phys. Rev. E* **68** (2003) 016404 .

19) Y. Kiwamoto, K. Ito, A. Sanpei, and M. Mohri: *Phys. Rev. Lett.* **85** (2000) 3173 .

20) Y. Soga, Y. Kiwamoto, A. Sanpei, and J. Aoki: *Phys. Plasmas* **10** (2003) 3922 .

21) D.D. Holm, J.E. Marsden, T. Ratiu, and A. Weinstein: *Phys. Rep.* **123** (1985) 1 .

22) R. C. Davidson: *Theory of Nonneutral Plasmas* (W. A. Benjamin, Inc., Reading, Mass., Tokyo, 1987).

23) J. Miller: *Phys. Rev. Lett.* **65** (1990) 2137 .

24) R. H. Kraichnan: *Phys. Fluids* **10** (1967) 1417 .

25) G. K. Batchelor: *Phys. Fluids* **12** (*Suppl. II*) (1969) 233 .

26) A. Leonard: *J. Comput. Phys.* **37** (1980) 288 .

27) C. K. Birdsall and A. B. Langdon: *Plasma Physics Via Computer Simulation* (Adam Hilger, Bristol, Philadelphia, New York, 1991).

28) W. H. Press, S. A. Tenkolsky, W. T. Vetterling, and B. P. Flannery: *Numerical Recipe in FORTRAN (Second Edition)* (Cambridge University Press, Cambridge, New York, Melbourne, 1992).

29) M.V. Melander, N.J. Zabusky, and J.C. McWilliams: *Phys. Fluids* **30** (1987) 2610 .

30) C. Anteneodo and C. Tsallis: *J. Molecular Liquids* **71** (1997) 255 .

